ACS OMEGA

http://pubs.acs.org/journal/acsodf

Article

Exploring the Influence of Engineering the Linker between the Donor and Acceptor Fragments on Thermally Activated Delayed Fluorescence Characteristics

Aftab Hussain,* Farah Kanwal,* Ahmad Irfan, Mehboob Hassan, and Jingping Zhang

Cite This: *ACS Omega* 2023, 8, 15638−15649

Read Online

ACCESS | Metrics & More | Article Recommendations | Supporting Information

ABSTRACT: We have expounded the unique molecular design architecture for efficient thermally activated delayed fluorescence (TADF) materials based on a donor−linker−acceptor−linker−donor (D−L−A−L−D) framework, which can be employed as predecessors of organic light-emitting diode (OLED) devices. Different from traditional donor−acceptor-type (D−A-type) TADF scaffolds, the D−L−A−L−D structural design avoids direct coupling amid the D and A fragments allowing the highest occupied molecular orbitals (HOMOs) and the lowest unoccupied molecular orbitals (LUMOs) to be spatially separated. It results in a reduced overlap between HOMOs and LUMOs, thus realizing fairly a slight singlet−triplet energy gap (ΔE_{ST}) and higher photoluminescence quantum yield (Φ). We revealed that manipulating a linker between D and A fragments in intramolecular charge transfer compounds is an auspicious approach for realizing small ΔE_{ST}. Herein, we report a group of organic electroluminescent D−L−A−L−D-type molecules with different electron-donating and electron-accepting moieties using density functional theory calculations and time-dependent density functional theory calculations. Two types of linkers, the π-conjugated phenylene ($-C_6H_4-$) and aliphatic alkyl chains or σ-spacer ($-CH_2-$ and $-CH_2-CH_2-$), were exploited between D and A fragments. In principle, the conjugation in D−π−A−π−D-type molecules and hyperconjugation in D−σ−A−σ−D type molecules encourage the spatial separation of the HOMO−LUMO causing a reduction in the ΔE_{ST}. All the designed molecules show a blue-shift in the emission wavelengths (λ_{em}) over the directly linked parent molecules except **DPA-DPS-C$_6$H$_4$** and **BTPA-DPS-C$_6$H$_4$** which show a red-shift. Violet-blue to green-yellow (376−566 nm) λ_{em} was observed from all of the investigated molecules. Other important properties that affect the efficiency of emission quantum yields like frontier molecular orbital analysis, natural population analysis, electron excitation analysis, exciton binding energies, ionization potentials, electronic affinities, and reorganization energies of the designed molecules were also inspected. We are confident that our work will effectively give a straightforward and distinctive approach to building incredibly effective TADF-OLEDs and a new perspective on their structural design.

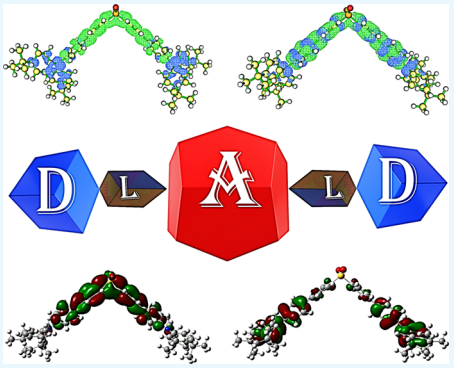

1. INTRODUCTION

At present, organic light-emitting diodes (OLEDs) are extensively exploited in solid-state lighting and high-resolution flat panel displays drawing significant interest in the industry as well as academia.[1,2] OLEDs employing noble-metal-based organometallic-phosphors can garner both singlet (25%) and triplet (75%) excitons via efficient spin−orbit coupling approaching external quantum efficiency (EQE) near to 100% in comparison with fluorescence-based OLEDs.[3−5] However, these precious-metal-based phosphors' high price, scarcity, high current density, and toxicity remain to be barriers to their use in many areas.[6−8] Effective OLEDs based on exciplex emitters and charge-transfer Cu(I) complexes have also drawn considerable attention, demonstrating an EQE as high as 16% in the past decades.[9−11] Recently, another auspicious pathway called thermally activated delayed fluorescence (TADF) has been in the spotlight as a viable substitute for phosphorescent materials. TADF materials are among the most auspicious classes of next-generation organic electroluminescent materials since they can theoretically realize an internal quantum efficiency (IQE) of ≈100% without the need for precious heavy metals.[2−4,12−15] In TADF emitters, the energy difference (ΔE_{ST}) between the lowest triplet (T_1) and the lowest singlet (S_1) excited state is very small, and an efficient upconversion from the T_1 state to S_1 state can take place to ensure effective reverse intersystem crossing (RISC) giving very high total singlet yields.[16−18] For efficient TADF scaffolds, a limited overlap between the highest occupied molecular orbitals and the lowest unoccupied molecular

Received: February 18, 2023
Accepted: April 6, 2023
Published: April 20, 2023

https://doi.org/10.1021/acsomega.3c01098
ACS Omega 2023, 8, 15638−15649

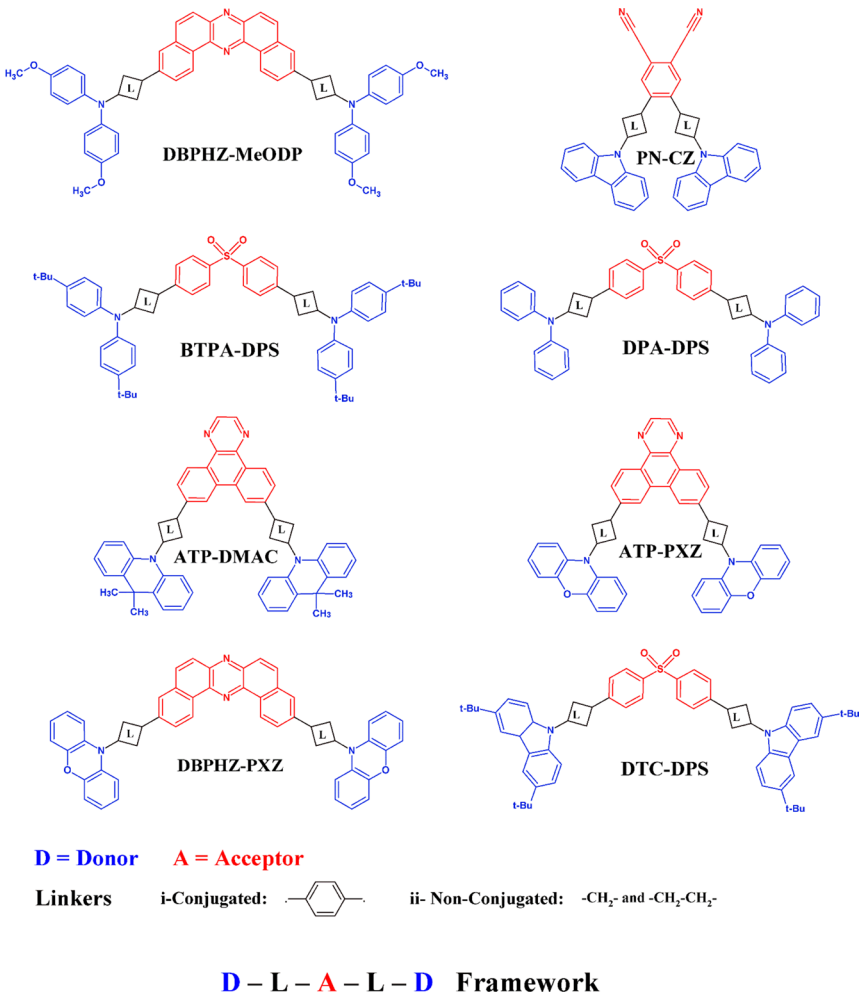

Figure 1. Scheme of the study showing eight parent compounds. Conjugated and nonconjugated linkers are employed between donor and acceptor fragments in the specified position to further design eight conjugated and eight nonconjugated derivatives.

orbitals (HOMOs and LUMOs) is a key factor for competent thermal upconversion through RISC thus realizing small ΔE_{ST}.[19,20] The excited states of conventional D−A-type TADF materials are charge transfer (CT) in nature where the HOMOs and the LUMOs are positioned on the D and the A part of the molecule, respectively.[2,18,21] The effective intramolecular charge transfer (ICT) character or spatial separation of HOMO−LUMO is mainly affected by the electron-donating and electron-withdrawing ability of D and A moieties in D−A topology, the dihedral angle between D−A units, spirojunction, homoconjugation, the length and the type of the linker between D and A fragments, etc.[22−25] Talking about the linker engineering between D and A units, a promising molecular design architecture for TADF materials so far is the D−π−A system (donor and acceptor moieties are connected via conjugated π-bonds) with twisted intramolecular charge transfer (TICT) characteristics and very infrequent D−σ−A type materials (donor and acceptor moieties are connected via nonconjugated σ-bonds) have also been studied.[24,26−29] In pursuit of the requirement to obtain high triplet energies bipolar hosts, the D−σ−A strategy has also been employed to restrict the conjugation and the electronic coupling between the D−A units. The device performances of D−σ−A emitters are still substandard than their D−π−A correspondents, and their lifetimes are not described yet.[30−33] Therefore, envisaging the prerequisite of D−A-separated conformation, it is rational to unite the D and A moieties with π-conjugated as well as with non-π-conjugated or σ-linker.

Herein, we report the successful transformation of fluorophores into a series of violet-blue to green-yellow TADF emitters by the manipulation of a linker (may be conjugated such as π-group or nonconjugated such as σ-bridge) within the molecular framework of the D−A structure. We have envisaged an upgraded molecular design architecture of the TADF molecules by using the D−L−A−L−D topology, where the linker controls the distance between D/A conformation in an intramolecular fashion.[34,35] In principle, the conjugation in D−π−A−π−D-type molecules[17,21,24,29] and hyperconjugation in D−σ−A−σ−D type molecules[2,36−39] encourages the spatial separation of the HOMOs and LUMOs, thus resulting in reduced ΔE_{ST}. Taking Dr. P. Data's and Adachi's reports as benchmark materials,[5,6,40,41] we have conceived some important D−L−A−L−D framework structures and examined their photophysical and electronic properties. In this study, different electron-donating and electron-accepting moieties were selected. Phenylene ($-C_6H_4-$) and methylene ($-CH_2-$ or ethylene $-CH_2-CH_2-$) groups have been opted as conjugated and non-conjugated linkers between the D and A parts, respectively. All of the investigated compounds are symmetric having C_2 symmetry whose chemical structures are displayed in Figure 1. We have thoroughly investigated the influences of the D−A

https://doi.org/10.1021/acsomega.3c01098
ACS Omega 2023, 8, 15638−15649

separation distance on the photophysical, electronic, and charge transfer properties of these molecules in terms of ΔE_{ST}, absorption and emission wavelength, Stokes shift, frontier molecular orbital analysis, population analysis, electron excitation analysis, exciton binding energies, charge injection and transport analysis which includes ionization potentials, electronic affinities, and hole−electron reorganization energies for the designed compounds to comprehend their properties for OLED application.

2. COMPUTATIONAL METHODOLOGY

All the calculations were computed using the Gaussian 09[42] program based on density functional theory and time-dependent density functional theory calculations. First of all, the ground-state geometry (S_0) optimization was accomplished using the most prevalent B3LYP/6-31g(d) method for the optimization. The vibrational frequency analysis was also done at the same theory level to confirm the equilibrium structure showing no imaginary frequency.[43−45] Then, after excited state optimization (S_1) at the same level, we performed functional analysis of the investigated molecules in toluene solvent employing various functionals like B3LYP, PBE0, M06, BMK, and ωB97XD as shown in Table S1. The M06 and BMK functionals showed close values to the experimental emission wavelength (λ_{em}) values and were chiefly selected to investigate the current systems.[5,6,40,41] The basis set effect was also observed using 6-31g(d), 6-31g(d,p), and 6-311+g(d,p) which showed almost similar results. Hence, the 6-31g(d) basis set was chosen for further calculations to save computational costs and resources. Then geometry optimizations of the ground states (S_0), singlet excited states (S_1), and triplet excited states (T_1) were performed. As seen from the S_0-optimized geometries, the HOMO and LUMO distributions of the studied molecules are chiefly dispersed asymmetrically over the D and A units, respectively.[46,47] The overlap (ρ) between the HOMO and the LUMO is undoubtedly diminished by the efficient partition of their electron densities due to the insertion of the linker (σ or π-bridge).[2,6] Furthermore, in comparison with the D−π−A−π−D type derivatives, the D−σ−A−σ−D type derivatives show a greater separation of the HOMOs and the LUMOs owing to the relatively large separation distance between the D and A moieties. This smaller ρ value signifies a smaller ΔE_{ST} value. The ΔE_{ST} values of all the molecules were calculated based on S_0-geometries when optimized by the TD-B3LYP/6-31g(d) method. Most of the calculations were performed in the gas phase but absorption and emission wavelengths were calculated in the toluene media using the polarizable continuum model (PCM). Violet-blue to green-yellow emission was observed for all of the investigated molecules. Postprocessing of results was done with Multiwfn, PyMOlyze, Origin, Gaussview, Gausssum software, etc.[5,36−39] In principle, the molecular energies of the lowest singlet excited states (E_S), as well as triplet excited states (E_T), are given by:

$$E_S = E + K + J \tag{1}$$

$$E_T = E + K - J \tag{2}$$

$$\Delta E_{ST} = E_S - E_T = 2J \tag{3}$$

which are dependent on the electron repulsion energies (K), orbital energies (E), and exchange energies (J) of two unpaired electrons at the singlet and triplet excited states, as revealed in eqs (1) and (2). The K, E, and J at the singlet and triplet excited states are similar to each other owing to the same electronic arrangement in one molecule. However, compared with increased E_S in S_1, the E_T is reduced in T_1 owing to the similar spin states of unpaired electrons; hence, ΔE_{ST} is twice of J. Since at S_1 and T_1 states, the two unpaired electrons are primarily dispersed over the frontier molecular orbitals, i.e., HOMOs and LUMOs, respectively, with the same J value. Hence, the J value of two electrons at HOMO and LUMO can be computed by:[29,35]

$$J = \iint \psi_L(1)\psi_H(2)\left(\frac{e^2}{r_1 - r_2}\right)\psi_L(2)\psi_H(1)\, dr_2\, dr_1 \tag{4}$$

where ψ_H and ψ_L denote the wave functions of the HOMO and LUMO, respectively, and e signifies the electronic charge. It is evident from eq 4 that ΔE_{ST} values increase with J values.

3. RESULTS AND DISCUSSION

3.1. ΔE_{ST} and HOMO−LUMO Overlap (ρ). Minimization of the ΔE_{ST} is the most necessitating parameter in the TADF development. Smaller the ΔE_{ST} value, higher would be the rate of RISC, and easier would be the upconversion of the excitons from T_1 to the S_1 state and ultimately to the S_0 state showing delayed fluorescence under thermal activation.[21,47] ΔE_{ST} is strongly dependent on spatial partitioning of the HOMO−LUMO, D−A orientation, and effective separation distance (R) between D and A units. There is an optimal value of R, depending on the size of the D and A units, to realize a large decay rate and small ΔE_{ST} simultaneously. To enrich the diversity of TADF molecules, many methods have been introduced to decrease ΔE_{ST}.[48] Herein, we are adopting the strategy of inserting a linker between the D and A parts of the molecule to examine the TADF properties of these devised molecules. The computed ΔE_{ST} values of these investigated molecules based on S_0 geometry using the TD-B3LYP/6-31g(d) method are recorded in Table 1 and are depicted in Figure 2. We have investigated that the ΔE_{ST} value declines by inserting the linker between the D and A units. It can be perceived from Table 1 that, compared to the parent compounds, all of the derived molecules exhibit relatively lower ΔE_{ST} values. In particular, manipulating a conjugated linker between D and A parts increases the effective separation distance between them which minimizes the ρ value and ultimately reduces the ΔE_{ST} value. Additionally, the non-conjugated linker further reduces the ΔE_{ST} values by controlling the conjugation length as this design strategy evades the effective electronic coupling between D−A resulting in further reduction of the ρ value.[49] In the case of **ATP-DMAC** and **ATP-PXZ**, we have introduced two $-CH_2-$ groups between D and A units as introducing one $-CH_2-$ group has increased the ΔE_{ST} value due to the increased ρ value. Furthermore, although the nonconjugated derivatives of **DTC-DPS** and **DBPHZ-PXZ** have higher ΔE_{ST} values than the conjugated derivatives, they have lower ΔE_{ST} values compared with the parent molecules depending upon the nature/size of D and A fragments. Moreover, ΔE_{ST} values are consistent with the ρ value and diminish as the ρ decreases. The ρ value decreases monotonically by inserting a linker between the D and A parts as compared to the parent molecules. Once more, the nonconjugated spacer is more effective in reducing the ρ value than that of the conjugated spacer ascribed to the extended D−A separation distance and

https://doi.org/10.1021/acsomega.3c01098
ACS Omega 2023, 8, 15638−15649

Table 1. Calculated HOMO−LUMO Overlap Values (ρ) in Whole Space Using the Multiwfn Analyzer and the ΔE_{ST} Values (in eV) of the Parent and Designed Molecules Based on S_0—State Geometries when Optimized Using the B3LYP/6-31g(d) Method

molecules	$E_S@S_0$ (eV)	$E_T@S_0$ (eV)	ΔE_{ST} (eV)	overlap (ρ)
DBPHZ-MeODP	2.4742	2.0982	0.3760	0.4973
DBPHZ-MeODP-C_6H_4	2.3741	2.1445	0.2296	0.2916
DBPHZ-MeODP-CH_2	2.2527	2.2369	0.0158	0.0973
PN-CZ	2.8386	2.4995	0.3391	0.4428
PN-CZ-C_6H_4	2.7425	2.5504	0.1921	0.2875
PN-CZ-CH_2	2.9739	2.9547	0.0192	0.1391
DPA-DPS	3.5328	2.8885	0.6443	0.6565
DPA-DPS-C_6H_4	3.1554	2.6583	0.4971	0.5034
DPA-DPS-CH_2	3.4049	3.2223	0.1826	0.1979
BTPA-DPS	3.4702	2.8608	0.6094	0.6514
BTPA-DPS-C_6H_4	3.0795	2.6188	0.4607	0.4910
BTPA-DPS-CH_2	3.2662	3.1457	0.1205	0.1938
ATP-DMAC	2.4397	2.4349	0.0048	0.0968
ATP-DMAC-C_6H_4	2.6298	2.6265	0.0033	0.0544
ATP-DMAC-CH_2	2.9432	2.8450	0.0982	0.0710
ATP-DMAC-2CH_2	2.8445	2.8436	0.0009	0.0401
ATP-PXZ	2.1516	2.1466	0.0050	0.0972
ATP-PXZ-C_6H_4	2.3398	2.3363	0.0035	0.0589
ATP-PXZ-CH2	2.6121	2.6039	0.0082	0.7358
ATP-PXZ-2CH_2	2.5929	2.5911	0.0018	0.0470
DTC-DPS	3.3027	2.9623	0.3404	0.4487
DTC-DPS-C_6H_4	3.1388	2.8310	0.3078	0.3385
DTC-DPS-CH_2	3.4765	3.1549	0.3216	0.1367
DBPHZ-PXZ	1.7854	1.7774	0.0080	0.1179
DBPHZ-PXZ-C_6H_4	1.9979	1.9968	0.0011	0.0426
DBPHZ-PXZ-CH_2	2.1930	2.1885	0.0045	0.0782

ineffective D−A electronic coupling. The ρ value is calculated by Becke's grid-based integration approach employing the given function in the Multiwfn program where i and j refer to the HOMO and LUMO, respectively.[50]

$$\rho = \int |\varphi_i(r)||\varphi_j(r)|dr \quad (5)$$

3.2. Photophysical Properties. The absorption (λ_{ab}) and emission (λ_{em}) wavelength values of all the studied molecules along with main configurations employing the TD-M06//TD-BMK/6-31g(d) level based on S_0 and S_1 state geometries, respectively, employing the PCM model in toluene media, are documented in Tables 2, 2S, and 3S and are portrayed in Figure 3. The Stokes-shift values were also documented in Table 2. As shown in Table 2, introducing the linker (conjugated or nonconjugated) between the D−A fragments leads to a bathochromic-shift or hypsochromic-shift in the λ_{ab} and λ_{em}.

From Table 2, we can see that for all the compounds the electronic shifts are of the $\pi \rightarrow \pi^*$ nature and the λ_{ab} bands originate from $S_0 \rightarrow S_1$ shifts which is chiefly the transfer of the electron from HOMO → LUMO[5] except for **ATP-PXZ-C_6H_4** and **DBPHZ-PXZ** for which the transfer of the electron is from the HOMO−1 to LUMO. By comparing the calculated λ_{ab} of the parent and designed molecules, it can be inferred that the λ_{ab} of almost all the designed molecules is blue-shifted as compared to the parent molecules because of the increase of the distance between D−A fragments except for the molecules **DPA-DPS-C_6H_4**, **BTPA-DPS-C_6H_4**, and **DPA-DPS-C_6H_4** which show a red-shift. The λ_{ab} of all the investigated molecules lies in the range of 329−482 nm, and the HOMO → LUMO transition ranges from 79−99%.

The emission color of the TADF materials depends upon the choice of the D and A moieties. In general, low electron-donating strength of D or high electron-accepting strength of A would lead to a blue emission and vice versa.[25] From Figure 3, we can see that all the investigated molecules show broad λ_{em} bands found in the range of 376−566 nm lying in the violet-blue to the green-yellow region of the electromagnetic spectrum. The LUMO → HOMO transition ranges from

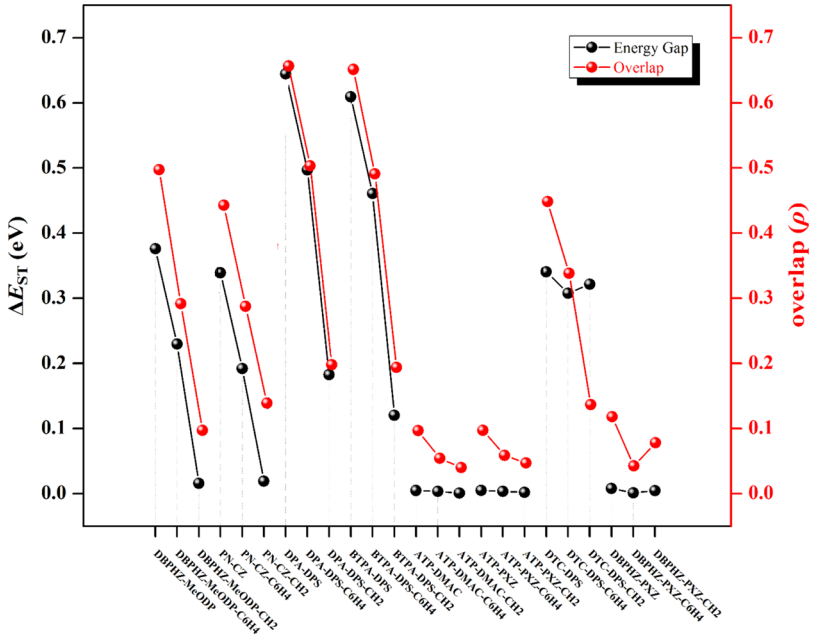

Figure 2. Relationship between singlet−triplet energy splitting (ΔE_{ST}) and HOMO−LUMO overlap (ρ) in whole space.

https://doi.org/10.1021/acsomega.3c01098
ACS Omega 2023, 8, 15638−15649

Table 2. Absorption (λ_{ab}) and Emission Wavelength (λ_{em}) of the Parent and Designed Molecules Containing Conjugated and Nonconjugated Linkers Based on Their S_0 and S_1 State, Respectively, Using the TD-M06//TD-BMK/6-31g(d) Method in Toluene Employing the PCM Model Along with Their Stokes-Shift Values ($\Delta\lambda = \lambda_{em} - \lambda_{ab}$)

molecules	λ_{ab} (nm)	main CI expansion/coefficient	λ_{em} (nm)	main CI expansion/coefficient	$\Delta\lambda$ (nm)
DBPHZ-MeODP	424	HOMO → LUMO (92%)	490	LUMO → HOMO (96%)	66
DBPHZ-MeODP-C_6H_4	408	HOMO → LUMO (80%)	444	LUMO → HOMO (90%)	36
DBPHZ-MeODP-CH_2	394	HOMO → LUMO (98%)	448	LUMO → HOMO (99%)	54
PN-CZ	371	HOMO → LUMO (97%)	488	LUMO → HOMO (98%)	117
PN-CZ-C_6H_4	357	HOMO → LUMO (91%)	393	LUMO → HOMO (93%)	36
PN-CZ-CH_2	335	HOMO → LUMO (99%)	376	LUMO → HOMO (99%)	41
DPA-DPS	348	HOMO → LUMO (91%)	416	LUMO → HOMO (93%)	68
DPA-DPS-C_6H_4	381	HOMO → LUMO (85%)	424	LUMO → HOMO (87%)	43
DPA-DPS-CH_2	339	HOMO → LUMO (92%)	403	LUMO → HOMO (94%)	64
BTPA-DPS	353	HOMO → LUMO (91%)	437	LUMO → HOMO (93%)	84
BTPA-DPS-C_6H_4	389	HOMO → LUMO (86%)	442	LUMO → HOMO (88%)	53
BTPA-DPS-CH_2	352	HOMO → LUMO (93%)	405	LUMO → HOMO (95%)	53
ATP-DMAC	440	HOMO → LUMO (90%)	495	LUMO → HOMO (97%)	55
ATP-DMAC-C_6H_4	409	HOMO → LUMO (80%)	448	LUMO → HOMO (93%)	39
ATP-DMAC-2CH_2	389	HOMO → LUMO (99%)	435	LUMO → HOMO (100%)	46
ATP-PXZ	482	HOMO → LUMO (91%)	566	LUMO → HOMO (97%)	84
ATP-PXZ-C_6H_4	446	HOMO−1 → LUMO (79%)	500	LUMO → HOMO (92%)	54
ATP-PXZ-2CH_2	416	HOMO → LUMO (99%)	484	LUMO → HOMO (100%)	68
DTC-DPS	358	HOMO → LUMO (92%)	421	LUMO → HOMO (94%)	63
DTC-DPS-C_6H_4	366	HOMO → LUMO (84%)	407	LUMO → HOMO (88%)	41
DTC-DPS-CH_2	329	HOMO → LUMO (95%)	393	LUMO → HOMO (96%)	64
DBPHZ-PXZ	452	HOMO−1 → LUMO (95%)	510	LUMO → HOMO (97%)	58
DBPHZ-PXZ-C_6H_4	401	HOMO → LUMO (90%)	441	LUMO → HOMO (95%)	40
DBPHZ-PXZ-CH_2	396	HOMO → LUMO (98%)	447	LUMO → HOMO (99%)	51

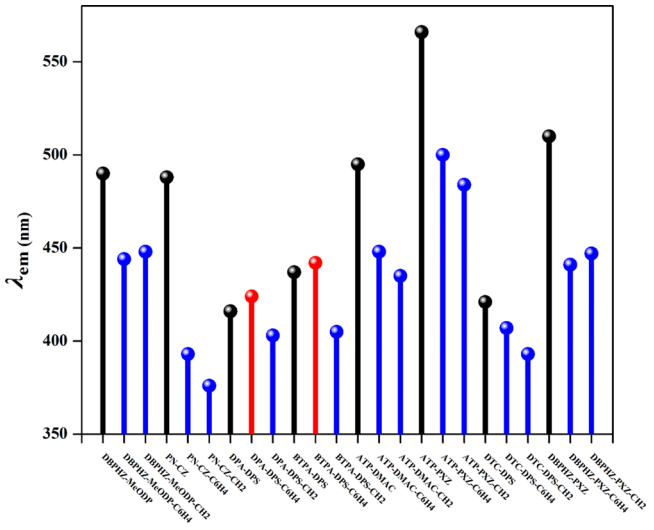

Figure 3. Emission wavelength (λ_{em}) of studied molecules under toluene solvent using the PCM model. Black, blue, and red colors represent parent molecules, designed molecules showing a blue-shift, and designed molecules showing a red-shift, respectively.

87−100%. All the designed molecules undoubtedly exhibit broad and featureless λ_{em} spectra, demonstrating that their S_1 excited states are characterized as ^{1}CT states, which is further validated by the frontier molecular orbital (FMO) spatial separation and electron−hole distribution.[51−54] The delayed fluorescent emission bands of the designed molecules are assigned to $\pi^* \rightarrow \pi$ electronic shifts, arising from the $S_1 \rightarrow S_0$ transition.[44] Comparing the calculated λ_{em} of the parent and designed molecules, it can be decided that almost all the designed molecules favor a blue-shift except for the molecules **DPA-DPS-C_6H_4** and **BTPA-DPS-C_6H_4** which show a red-shift due to the structural reorganization during the excitation.

The Stokes shift is the difference amongst the positions of the λ_{ab} and λ_{em} band maxima of similar electronic shifts. It is shown in Table 2 that all the devised molecules show a smaller Stokes shift as compared to the parent molecules except **DTC-DPS-CH_2**. The introduction of the linker (both conjugated and nonconjugated) was advantageous to decrease the Stokes shift and enhance PLQY. The Stokes-shift values were reduced more when inserting a conjugated linker compared with nonconjugated. The larger Stokes shift ascribes to large geometry distortion from the $S_0 \rightarrow S_1$ state of the studied molecules. PN-CZ possesses the largest Stokes shift implying that it undergoes a substantial structural reorganization in the excited state owing to π-conjugation length and ICT from the CZ donor to the PN acceptor unit.[44,55]

3.3. FMO Analysis. It is a renowned verity that the frontier molecular orbitals (HOMO and LUMO) provide useful pieces of information regarding the TADF characteristics. We have portrayed the HOMO−LUMO spatial distribution of all the studied molecules at S_0 state in Figures 4 and S1. It is obvious that in the case of the parent molecules, the HOMOs are mainly dispersed on the D fragments and partially on the A moiety while the LUMOs are predominantly localized on the A and slightly on the D moieties. Inserting a linker between the D and A fragments enlarges the D−A separation distance leading to a smaller ρ value showing a clear separation between them as compared to the parent molecule resulting in a smaller ΔE_{ST} value. As portrayed in Figures 4 and S1, for the compounds containing conjugated linkers, the major donation of HOMO comes from the D fragments and a slight donation from the central phenyl linker. Also, the LUMO distributions principally confine to the A moiety and partly extend to the

https://doi.org/10.1021/acsomega.3c01098
ACS Omega 2023, 8, 15638−15649

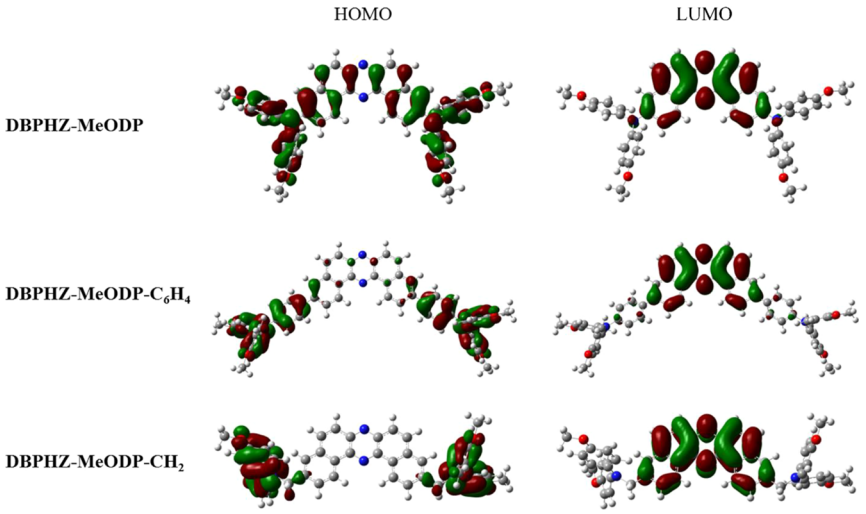

Figure 4. HOMO−LUMO spatial distribution calculated using B3LYP/6-31g(d) at S_0 state. The isosurface value for FMOs is 0.02.

central phenyl ring. Alternatively, the nonconjugated linker constrains the delocalization of the π-electronic cloud and displays a greater separation of HOMOs and LUMOs, confining them largely on D and A parts, respectively, because of the relatively smaller ρ value and hence is more effective than that of the conjugated linker resulting in a more pronounced reduction in the ΔE_{ST} value.[19,21,44]

We have also analyzed the density of states (DOS) spectrum to reinforce the effect of HOMO−LUMO separations as shown in Figure S2. The DOS spectrum clearly shows that the HOMOs are chiefly located on the D moiety, while the LUMOs reside on the A fragment. This indicates the effective separation between D and A moieties, reflecting the characteristics of potential TADF.[43,44,50] Moreover, we have calculated the overlap value of the electron densities of HOMOs and LUMOs between different D and A fragments using the PyMOlyze software as shown in Table S4 and portrayed in Figure S3. The overlap values lie in the range of 0.003 → 0.044. This small overlap value indicates that the transitions from HOMO to LUMO have a small electron exchange energy and a strong CT character, thus leading to a fairly small ΔE_{ST} to engender TADF. Table S4 also indicates that these overlap values are reduced by inserting a spacer between D and A fragments. In addition, there is no overlap between D fragments meaning that D fragments are clearly separated from each other.[24,46,56] The percentage of electronic distribution of HOMOs and LUMOs on different D and A fragments has also been calculated via Mulliken Population Analysis (MPA) and Modified Mulliken Population Analysis also called C-Squared Population Analysis (SCPA) using the PyMOlyze software as shown in Tables S5 and S6, respectively. These values show that by inserting a linker between D and A fragments, the LUMO distribution of A fragments is increased with a corresponding decrease in the LUMO distribution of the D part and vice versa.[50,56−59]

3.4. Natural Population Analysis (NPA) and the ΔE_{ST}.

The NPA method is used to compute atomic charges as well as orbital populations of molecular wave functions. The NPA is an alternate method to the traditional MPA and is based on natural atomic orbitals (NAOs) for a certain molecule in any arbitrary atomic orbital. It demonstrates the upgraded numerical stability and explains the electronic dispersal in molecules of high ionic characters in a superior way.[24,57−59]

Using the NPA method, we have computed the atomic charges of the studied molecules in the S_0 and S_1 states to comprehend the relationship between the ΔE_{ST} and the NPA charge difference between the ground state and excited state ($\Delta Q = Q_{S0} - Q_{S1}$) as shown in Table S7 and displayed in Figure 5. It

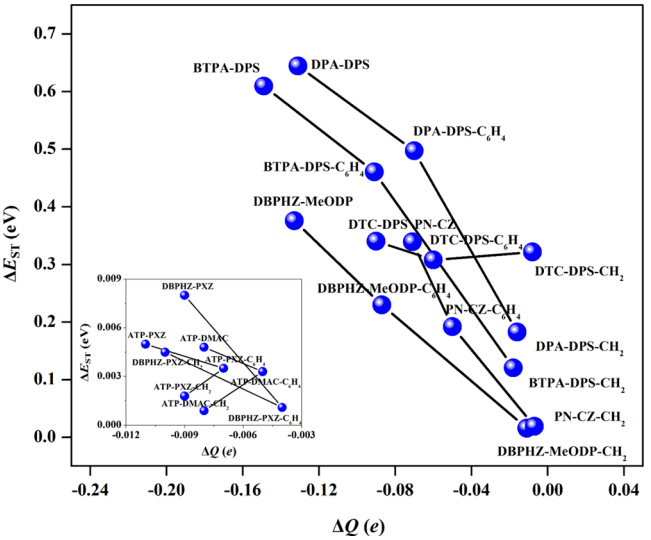

Figure 5. ΔE_{ST} values as a function of NPA charge difference ($\Delta Q = Q_{S0} - Q_{S1}$) on the acceptor fragment.

is obvious that for the S_0 and S_1 states of all the investigated molecules, the A fragments hold a positive charge while the D moieties have a negative charge. However, the ΔQ values of the A fragments are negative, indicating that the A fragments accept electrons in the shift from S_1 to S_0. Contrarily, the ΔQ value is positive for the D fragments (D1/D2), indicating that the D fragments donated electrons in this transition process. The ΔE_{ST} values alter with the ΔQ values on the D and A fragments and diminish with increased ΔQ value on the A fragment. It is shown that the introduction of the linker between the D and A fragments leads to a reduction in ΔE_{ST} value due to increased ΔQ value on the A fragment, which is further reduced by the nonconjugated linker compared with conjugated. Although the conjugated derivatives of **ATP-DMAC**, **ATP-PXZ**, and **DBPHZ-PXZ** have higher ΔQ values

https://doi.org/10.1021/acsomega.3c01098
ACS Omega 2023, 8, 15638−15649

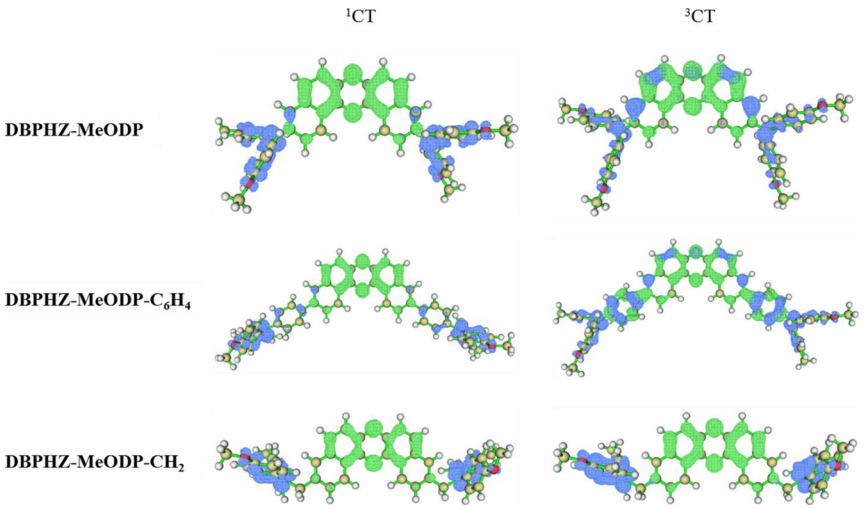

Figure 6. Hole and electron distributions in the first singlet excited and selected triplet states (^{1}CT and ^{3}CT) for the investigated molecules. Blue and green iso-surfaces represent hole and electron distributions, respectively.

on the A fragment compared with the parent molecules but talking about their nonconjugated derivatives, the **ATP-DMAC-CH$_2$** has the same value of ΔQ on the A fragment as the parent molecule, the **ATP-PXZ-CH$_2$** has a lower ΔQ value than the conjugated part but higher than the parent molecule and **DBPHZ-PXZ-CH$_2$** has a lower value of ΔQ value even than the parent molecule.

3.5. Electron Excitation Analysis (Transition Characteristics). We have investigated the electron−hole distributions of the first singlet (S_1) excited state and selected triplet excited states using the Multiwfn program to figure out the excitation properties (transition character) of the electrons at various excited states as shown in Figures 6 and S4. The calculated results show that the S_1 states of all the investigated molecules and triplet excited states of the majority of the molecules are CT in nature due to the distributions of hole and electron at D and A parts of the compounds, respectively. The singlet and triplet state geometries for almost all of the compounds are similar to each other showing an easy upconversion process from the T_1 state to the S_1 state except for **BTPA-DPS-CH$_2$-T$_1$** and **DTC-DPS-CH$_2$-T$_7$** whose triplet states are different from the singlet ones.[46,47,50]

3.6. Exciton Binding Energy (E_b). In order to comprehend the optoelectronic properties of OLEDs, the exciton binding energy (E_b) is an additional important parameter. It is an essential element of the electroluminescence quantum efficiency of OLEDs[60,61] which can be determined by the following equation:

$$E_b = \Delta E_{L-H} - E_{flu} \quad (6)$$

From eq 6, it was perceived that E_b depends on the electrical band gap or transport gap which corresponds to the HOMO−LUMO energy difference, and the optical band gap which corresponds to the fluorescence energy (E_{flu}). E_b measures the Coulomb interactions between a hole and an electron and helps us to understand the attraction−repulsion interactions between them. An exciton maybe demonstrated as a two-particle system: when an electron is raised into the LUMO, it leaves behind the hole in the HOMO.[35,62,63] Usually, a larger E_b is necessary for OLED materials to enhance the possibility of recombination of electron−hole pair. If $E_b \gg k_{BT}$ (thermal energy, i.e., the average energy of the molecule at room temperature ≈25−27 meV), the bound excitons are stable. Contrarily, if $k_{BT} \gg E_b$, the excitons are unstable, they can decay into charged polaron pairs.[35,63,64] It is obvious from Figure 7 and Table S8 that all the investigated molecules have

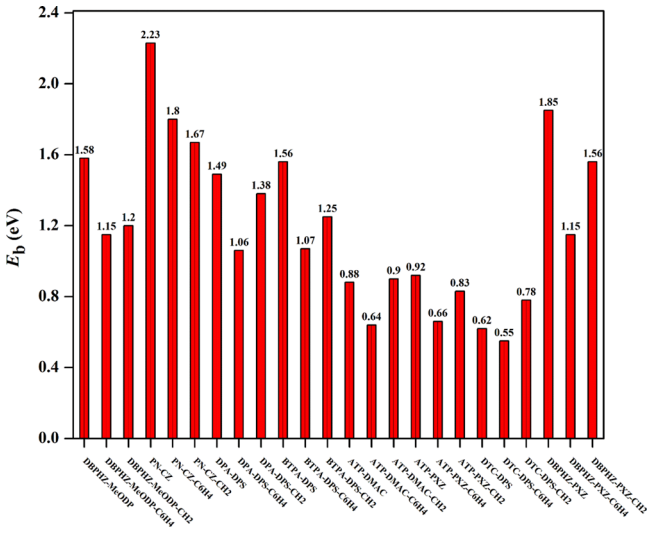

Figure 7. Exciton binding energy (E_b) of all the investigated molecules.

large E_b ($E_b \geq k_{BT}$) permitting the photoemission at room temperature. Furthermore, the molecules containing non-conjugated linkers have larger E_b values than that of conjugated linkers except for **ATP-DMAC-CH$_2$** and **DTC-DPS-CH$_2$** which have higher E_b values. It indicates the easier formation of the exciton in the OLEDs and hence higher fluorescent quantum efficiency.

3.7. Charge Injection and Transport Analysis. The charge injection and transport characteristics of the OLED device may have an impact on its performance. We have calculated the vertical and adiabatic ionization potentials (IP_v and IP_a), vertical and adiabatic electronic affinities (EA_v and EA_a), the hole extraction potential (HEP), and the electron extraction potential (EEP) using the potential energy surface (PES) method in order to determine the charge injection and transport features as listed in Table S9. The ionization

https://doi.org/10.1021/acsomega.3c01098
ACS Omega 2023, 8, 15638−15649

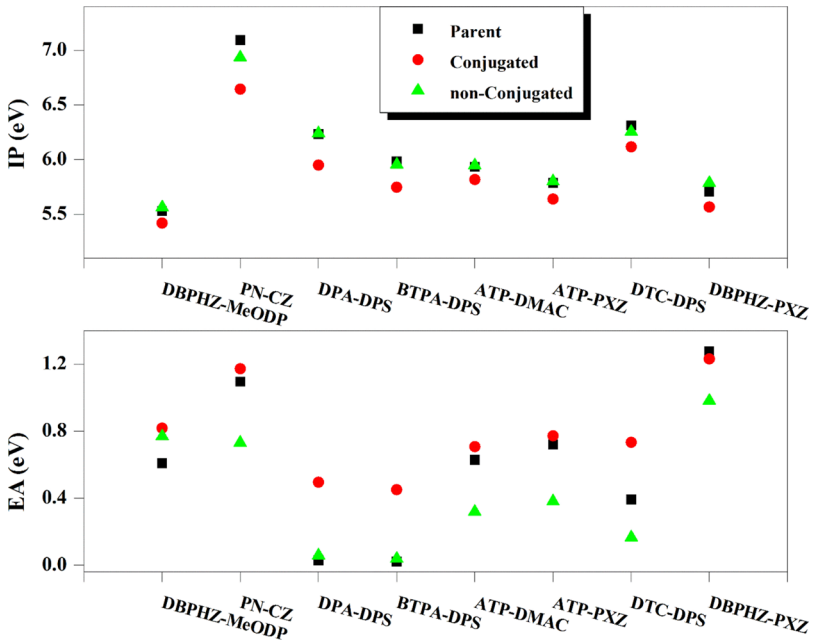

Figure 8. Ionization potentials (IP_v) and electronic affinities (EA_v) values for all the investigated molecules.

potentials and electronic affinities are exploited to evaluate the energy barrier for the hole/electron injection capabilities of molecules. Generally, the lower IP and the higher EA imply the easier injection of electrons/holes from the electron/hole transport host material to the emitter.[24,35,65] Figure 8 clearly shows that the designed compounds containing conjugated linkers have lower IP_v values and higher EA_v values than that of the parent compounds indicating the superior hole and electron injection capacity of the materials, respectively. The conjugated linker increases the HOMO energy level, hence favoring the easy ejection of electrons. However, in the case of the designed compounds containing nonconjugated linkers, **ATP-DMAC-2CH$_2$**, **ATP-PXZ-2CH$_2$**, and **DBPHZ-PXZ-CH$_2$** have shown the opposite trend of both IP and EA compared to the conjugated linkers. Likewise, **DBPHZ-MeODP-CH$_2$** and **DPA-DPS-CH$_2$** also have higher IP values and **PN-CZ-CH$_2$** and **DTC-DPS-CH$_2$** have lower EA values compared to the parent molecules showing the reverse trend.

There are two utmost models available theoretically for the transference of charge carriers in organic molecules: hopping and band-like. Likewise, there are two most widely applied charge transfer rate theories called Fermi's golden rule (FGR) and the Marcus theory.[66,67] The intermolecular transport of hole and electron is symbolized by the following equation:

$$M^{+/-} + M^{*} = M + M^{*+/-} \tag{7}$$

where $M^{+/-}$ represents the species in the cationic/anionic state, and M* is the adjacent neutral species. As stated by the Marcus/Hush theory, in the high temperature as well as stronger coupling limits, the hole/electron transfer rate (k) can be evaluated by the following formula:

$$k = Ae^{-\lambda/4k_bT} \tag{8}$$

where "A" is a prefactor that affects the electronic coupling of nearby molecules, k_b is the Boltzmann constant, T is the temperature, and λ is the reorganization energy associated with geometric relaxation escorting charge transfer. The λ is one of the two important elements that affect the charge transfer rate with the other being intermolecular charge transfer integral (V). The λ is a significant element that governs the efficiency of OLED materials and links the electronic structures and the charge transport properties. The internal hole/electron reorganization energies using the potential energy surface (PES) method (the other being the normal mode method) can be expressed by the following equations:[63,68−72]

$$\lambda_h = \lambda_+ + \lambda_0 = [E^+(M) - E^+M^+] + [E(M^+) - EM] = IP_V - HEP \tag{9}$$

$$\lambda_e = \lambda_- + \lambda_0 = [E^-(M) - E^-M^-] + [E(M^-) - EM] = EEP - EA_V \tag{10}$$

where $E(M^-)$ and $E(M^+)$ are the energies of neutral species at the optimized charged state, and $E^-(M^-)$ and $E^+(M^+)$ are the energies of charged molecules at the optimized charged state.

According to the Marcus theory, a smaller reorganization energy value (both λ_h and λ_e) is required for an effective charge transfer. It can be perceived from Figure S5 and Table S9 that the calculated λ_e values for the majority of the designed molecules are smaller than the parent compounds but are larger than the classical electron transport material tri(8-hydroxyquinolinato) aluminum(III) (0.28 eV). In contrast, the calculated λ_h values for all the studied molecules are lower than the typical hole transport material *N*,*N*′-diphenyl-*N*,*N*-bis(3-methyl-phenyl)-(1,10-biphenyl)-4,4′-diamine (TPD, 0.29 eV).[21,73] Compared to the molecules containing nonconjugated linker, most of the conjugated linker-containing molecules exhibits lower reorganization energies (both λ_h and λ_e). However, the λ_h of designed molecules containing a nonconjugated linker is larger than that of the parent molecules but still less than the typical hole transport material. We can also observe that λ_h is found to be lower compared with λ_e, demonstrating that the hole transport capacity of these designed materials is superior to electron transporting ability. Moreover, an efficient emitting material requires lower ΔE values ($\Delta E = \lambda_e - \lambda_h$ is the modulus of the energy difference

https://doi.org/10.1021/acsomega.3c01098
ACS Omega 2023, 8, 15638−15649

between the electrons and holes).[35] As it is obvious from Figure 9 that the insertion of the linker (conjugated or nonconjugated) between the D and A moiety has resulted in a reduction in the ΔE values compared to the parent compounds except **ATP-PXZ-2CH$_2$**.

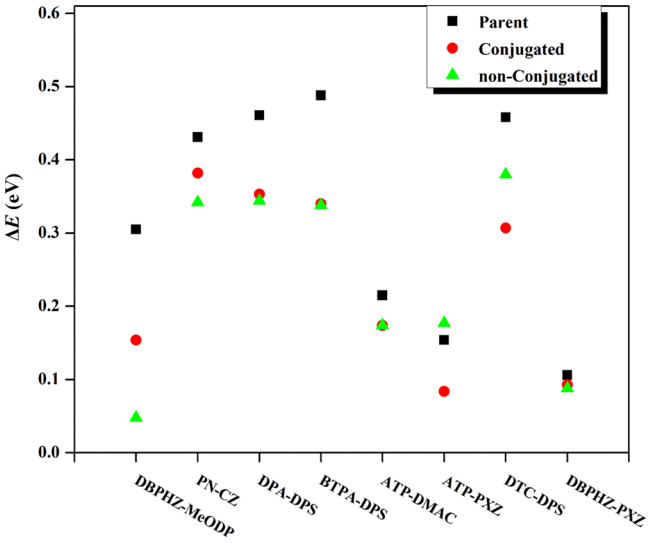

Figure 9. Reorganization energy difference between holes and electrons (λ_h and λ_e) for all the investigated molecules.

4. CONCLUSIONS

In short, we have proposed a unique molecular design concept (D−L−A−L−D) for TADF emitters by inserting a linker (σ or π-spacer) between electron-donating and electron-accepting moieties. Decreasing ΔE_{ST} without increasing the HOMO−LUMO overlap is a key factor in the realization of proficient TADF emitters. Herein, we have achieved this goal by inserting a linker between D and A which enlarges the effective separation distance (R) between D and A to realize large radiative efficiency and small ΔE_{ST} simultaneously. The nonconjugated spacer was realized to be more effective in lowering the ΔE_{ST} value compared to the conjugated one since it blocks the electronic communication between the HOMO−LUMO more efficiently than the conjugated linker. The photophysical spectra revealed that all the designed molecules exhibit broad and featureless λ_{em} spectra displaying blue-shift. The introduction of the linker has finely tuned the λ_{em} color from violet-blue to green-yellow (376−566 nm) with reasonable LUMO to HOMO transition (87−100%) depending upon electron-donating and electron-accepting strength of D and A moieties. The results of the NPA method showed that the introduction of the linker between D and A units decreases the ΔE_{ST} value, and these outcomes are consistent with the aforementioned results. The electron excitation analysis confirmed the CT nature of the singlet and triplet excited states. Similar geometries at S_1 and T_1 for almost all the compounds showed an easy upconversion from T_1 to the S_1 state. All the investigated molecules have large exciton binding energy ($E_b \geq k_{BT}$) permitting photoemission even at room temperature. The IP and EA data showed that the conjugated linker was more effective compared with the nonconjugated linker in lowering IP values and enhancing the EA values indicating their superior hole/electron injection capacity. From the reorganization energy values, we observed that compared to the molecules containing nonconjugated linkers, most of the conjugated linker-containing molecules exhibit lower reorganization energies (both λ_h and λ_e). The ΔE values of almost all designed molecules are also lower compared to the parent molecules. Furthermore, the λ_h values of all the studied molecules are less than the typical hole transport material and also lower compared with λ_e, demonstrating that our designed molecules are better hole transport materials. All these results show that the D−L−A−L−D-type design strategy could be another effectual choice for realizing efficient TADF emitters in the future. Hence, we believe that the incorporation of the linker between D and A moiety is a propitious strategy for the construction of incredibly effective TADF-OLEDs and a new perspective on their structural design.

■ ASSOCIATED CONTENT

Supporting Information

The Supporting Information is available free of charge at https://pubs.acs.org/doi/10.1021/acsomega.3c01098.

Absorption, emission, DOS spectrum, HOMO−LUMO spatial distribution, overlap of electronic transition density of HOMOs and LUMOs between different Donors and Acceptor units, overlap population density diagram, percentage of electronic distribution of HOMOs and LUMOs on different donors and acceptor fragments calculated via Mulliken Population Analysis and SCPA, atomic charges calculated using the NPA method, Exciton binding energy, vertical and adiabatic ionization potentials, electronic affinities, hole and electron extraction potentials, hole and electron reorganization energies, percentage of CT characters, and contribution of various molecular orbitals to hole−electron distribution (PDF)

■ AUTHOR INFORMATION

Corresponding Authors

Aftab Hussain − *School of Chemistry, University of the Punjab, Lahore 54590, Pakistan;* orcid.org/0000-0001-9741-4864; Phone: +923426224761; Email: aftab.chem@pu.edu.pk

Farah Kanwal − *School of Chemistry, University of the Punjab, Lahore 54590, Pakistan*; Email: farahkchem@yahoo.com

Authors

Ahmad Irfan − *Department of Chemistry, College of Science, King Khalid University, Abha 61413, Saudi Arabia*

Mehboob Hassan − *Department of Chemistry, University of Narowal, Narowal, Punjab 51600, Pakistan*

Jingping Zhang − *Faculty of Chemistry, Northeast Normal University, Changchun 130024, China*

Complete contact information is available at: https://pubs.acs.org/10.1021/acsomega.3c01098

Author Contributions

A.H.: conceptualization, data curation, investigation, methodology, and writing-original draft; F.K.: validation and writing-original draft; A.I.: data curation, formal analysis, and writing-review and editing; M.H.: validation and writing-original draft; J.Z.: supervision, validation, writing-original draft, and data curation.

Notes

The authors declare no competing financial interest.

https://doi.org/10.1021/acsomega.3c01098
ACS Omega 2023, 8, 15638−15649

■ ACKNOWLEDGMENTS

A.I. extends his appreciation to the Deanship of Scientific Research at King Khalid University through large group Research Project under grant number RGP2/63/44.

■ REFERENCES

(1) Zhang, Q.; Li, B.; Huang, S.; Nomura, H.; Tanaka, H.; Adachi, C. Efficient blue organic light-emitting diodes employing thermally activated delayed fluorescence. *Nat. Photonics* **2014**, *8*, 326−332.
(2) Geng, Y.; D'Aleo, A.; Inada, K.; Cui, L.-S.; Kim, J. U.; Nakanotani, H.; Adachi, C. Donor−σ−Acceptor Motifs: Thermally Activated Delayed Fluorescence Emitters with Dual Upconversion. *Angew. Chem., Int. Ed.* **2017**, *56*, 16536−16540.
(3) Adachi, C.; Baldo, M. A.; Thompson, M. E.; Forrest, S. R. Nearly 100% internal phosphorescence efficiency in an organic light-emitting device. *J. Appl. Phys.* **2001**, *90*, 5048−5051.
(4) Hamze, R.; Shi, S.; Kapper, S. C.; Muthiah Ravinson, D. S.; Estergreen, L.; Jung, M. C.; Tadle, A. C.; Haiges, R.; Djurovich, P. I.; Peltier, J. L.; Jazzar, R.; Bertrand, G.; Bradforth, S. E.; Thompson, M. E. "Quick-Silver" from a Systematic Study of Highly Luminescent, Two-Coordinate, d(10) Coinage Metal Complexes. *J. Am. Chem. Soc.* **2019**, *141*, 8616−8626.
(5) Zhang, Q.; Li, J.; Shizu, K.; Huang, S.; Hirata, S.; Miyazaki, H.; Adachi, C. Design of efficient thermally activated delayed fluorescence materials for pure blue organic light emitting diodes. *J. Am. Chem. Soc.* **2012**, *134*, 14706−14709.
(6) Uoyama, H.; Goushi, K.; Shizu, K.; Nomura, H.; Adachi, C. Highly efficient organic light-emitting diodes from delayed fluorescence. *Nature* **2012**, *492*, 234−238.
(7) Hirai, M.; Tanaka, N.; Sakai, M.; Yamaguchi, S. Structurally Constrained Boron-, Nitrogen-, Silicon-, and Phosphorus-Centered Polycyclic pi-Conjugated Systems. *Chem. Rev.* **2019**, *119*, 8291−8331.
(8) Cui, L. S.; Nomura, H.; Geng, Y.; Kim, J. U.; Nakanotani, H.; Adachi, C. Controlling Singlet-Triplet Energy Splitting for Deep-Blue Thermally Activated Delayed Fluorescence Emitters. *Am. Ethnol.* **2017**, *56*, 1571−1575.
(9) Zhang, Q.; Zhou, Q.; Cheng, Y.; Wang, L.; Ma, D.; Jing, X.; Wang, F. Highly Efficient Electroluminescence from Green-Light-Emitting Electrochemical Cells Based on CuI Complexes. *Adv. Funct. Mater.* **2006**, *16*, 1203−1208.
(10) Deaton, J. C.; Switalski, S. C.; Kondakov, D. Y.; Young, R. H.; Pawlik, T. D.; Giesen, D. J.; Harkins, S. B.; Miller, A. J. M.; Mickenberg, S. F.; Peters, J. C. E-Type Delayed Fluorescence of a Phosphine-Supported Cu2(μ-NAr2)2 Diamond Core: Harvesting Singlet and Triplet Excitons in OLEDs. *J. Am. Chem. Soc.* **2010**, *132*, 9499−9508.
(11) Zhang, Q.; Komino, T.; Huang, S.; Matsunami, S.; Goushi, K.; Adachi, C. Triplet Exciton Confinement in Green Organic Light-Emitting Diodes Containing Luminescent Charge-Transfer Cu(I) Complexes. *Adv. Funct. Mater.* **2012**, *22*, 2327−2336.
(12) Hatakeyama, T.; Shiren, K.; Nakajima, K.; Nomura, S.; Nakatsuka, S.; Kinoshita, K.; Ni, J.; Ono, Y.; Ikuta, T. Ultrapure Blue Thermally Activated Delayed Fluorescence Molecules: Efficient HOMO-LUMO Separation by the Multiple Resonance Effect. *Adv. Mater.* **2016**, *28*, 2777−2781.
(13) Cui, L. S.; Kim, J. U.; Nomura, H.; Nakanotani, H.; Adachi, C. Benzimidazobenzothiazole-Based Bipolar Hosts to Harvest Nearly All of the Excitons from Blue Delayed Fluorescence and Phosphorescent Organic Light-Emitting Diodes. *Am. Ethnol.* **2016**, *55*, 6864−6868.
(14) Lin, T. A.; Chatterjee, T.; Tsai, W. L.; Lee, W. K.; Wu, M. J.; Jiao, M.; Pan, K. C.; Yi, C. L.; Chung, C. L.; Wong, K. T.; Wu, C. C. Sky-Blue Organic Light Emitting Diode with 37% External Quantum Efficiency Using Thermally Activated Delayed Fluorescence from Spiroacridine-Triazine Hybrid. *Adv. Mater.* **2016**, *28*, 6976−6983.
(15) Wang, Y. K.; Wu, S. F.; Yuan, Y.; Li, S. H.; Fung, M. K.; Liao, L. S.; Jiang, Z. Q. Donor-sigma-Acceptor Molecules for Green Thermally Activated Delayed Fluorescence by Spatially Approaching Spiro Conformation. *Org. Lett.* **2017**, *19*, 3155−3158.
(16) Dias, F. B.; Bourdakos, K. N.; Jankus, V.; Moss, K. C.; Kamtekar, K. T.; Bhalla, V.; Santos, J.; Bryce, M. R.; Monkman, A. P. Triplet harvesting with 100% efficiency by way of thermally activated delayed fluorescence in charge transfer OLED emitters. *Adv. Mater.* **2013**, *25*, 3707−3714.
(17) Zhang, Q.; Kuwabara, H.; Potscavage, W. J., Jr.; Huang, S.; Hatae, Y.; Shibata, T.; Adachi, C. Anthraquinone-based intramolecular charge-transfer compounds: computational molecular design, thermally activated delayed fluorescence, and highly efficient red electroluminescence. *J. Am. Chem. Soc.* **2014**, *136*, 18070−18081.
(18) Shizu, K.; Tanaka, H.; Uejima, M.; Sato, T.; Tanaka, K.; Kaji, H.; Adachi, C. Strategy for Designing Electron Donors for Thermally Activated Delayed Fluorescence Emitters. *J. Phys. Chem. C* **2015**, *119*, 1291−1297.
(19) Samanta, P. K.; Kim, D.; Coropceanu, V.; Brédas, J.-L. Up-Conversion Intersystem Crossing Rates in Organic Emitters for Thermally Activated Delayed Fluorescence: Impact of the Nature of Singlet vs Triplet Excited States. *J. Am. Chem. Soc.* **2017**, *139*, 4042−4051.
(20) Tu, Z.; Han, G.; Hu, T.; Duan, R.; Yi, Y. Nature of the Lowest Singlet and Triplet Excited States of Organic Thermally Activated Delayed Fluorescence Emitters: A Self-Consistent Quantum Mechanics/Embedded Charge Study. *Chem. Mater.* **2019**, *31*, 6665−6671.
(21) Gao, Y.; Geng, Y.; Wu, Y.; Zhang, M.; Su, Z.-M. Investigation on the effect of connected bridge on thermally activated delayed fluorescence property for DCBPy emitter. *Dyes Pigm.* **2017**, *145*, 277−284.
(22) Li, W.; Li, B.; Cai, X.; Gan, L.; Xu, Z.; Li, W.; Liu, K.; Chen, D.; Su, S. J. Tri-Spiral Donor for High Efficiency and Versatile Blue Thermally Activated Delayed Fluorescence Materials. *Angew. Chem., Int. Ed.* **2019**, *58*, 11301−11305.
(23) Kawasumi, K.; Wu, T.; Zhu, T.; Chae, H. S.; Van Voorhis, T.; Baldo, M. A.; Swager, T. M. Thermally Activated Delayed Fluorescence Materials Based on Homoconjugation Effect of Donor-Acceptor Triptycenes. *J. Am. Chem. Soc.* **2015**, *137*, 11908−11911.
(24) Lu, J.; Zheng, Y.; Zhang, J. Rational design of phenoxazine-based donor-acceptor-donor thermally activated delayed fluorescent molecules with high performance. *Phys. Chem. Chem. Phys.* **2015**, *17*, 20014−20020.
(25) Oh, C. S.; Pereira, D. S.; Han, S. H.; Park, H. J.; Higginbotham, H. F.; Monkman, A. P.; Lee, J. Y. Dihedral Angle Control of Blue Thermally Activated Delayed Fluorescent Emitters through Donor Substitution Position for Efficient Reverse Intersystem Crossing. *ACS Appl. Mater. Interfaces* **2018**, *10*, 35420−35429.
(26) Ban, X.; Jiang, W.; Lu, T.; Jing, X.; Tang, Q.; Huang, S.; Sun, K.; Huang, B.; Lin, B.; Sun, Y. Self-host thermally activated delayed fluorescent dendrimers with flexible chains: an effective strategy for non-doped electroluminescent devices based on solution processing. *J. Mater. Chem. C* **2016**, *4*, 8810−8816.
(27) Godumala, M.; Choi, S.; Kim, H. J.; Lee, C.; Park, S.; Moon, J. S.; Si Woo, K.; Kwon, J. H.; Cho, M. J.; Choi, D. H. Novel dendritic large molecules as solution-processable thermally activated delayed fluorescent emitters for simple structured non-doped organic light emitting diodes. *J. Mater. Chem. C* **2018**, *6*, 1160−1170.
(28) Li, C.; Du, X.; Zhou, Y.; Ye, J.; Fu, L.; Humphrey, M. G.; Wu, C.; Zhao, J.; Du, Y.; Tao, S.; Wu, J.; Zhang, C. A simple and broadly applicable synthesis of fluorene-coupled D−σ−A type molecules: towards high-triplet-energy bipolar hosts for efficient blue thermally-activated delayed fluorescence. *J. Mater. Chem. C* **2018**, *6*, 6949−6957.
(29) Tao, Y.; Yuan, K.; Chen, T.; Xu, P.; Li, H.; Chen, R.; Zheng, C.; Zhang, L.; Huang, W. Thermally activated delayed fluorescence materials towards the breakthrough of organoelectronics. *Adv. Mater.* **2014**, *26*, 7931−7958.
(30) Mehes, G.; Nomura, H.; Zhang, Q.; Nakagawa, T.; Adachi, C. Enhanced electroluminescence efficiency in a spiro-acridine derivative through thermally activated delayed fluorescence. *Angew. Chem., Int. Ed.* **2012**, *51*, 11311−11315.

https://doi.org/10.1021/acsomega.3c01098
ACS Omega 2023, 8, 15638−15649

(31) Fan, C.; Chen, Y.; Liu, Z.; Jiang, Z.; Zhong, C.; Ma, D.; Qin, J.; Yang, C. Tetraphenylsilane derivatives spiro-annulated by triphenylamine/carbazole with enhanced HOMO energy levels and glass transition temperatures without lowering triplet energy: host materials for efficient blue phosphorescent OLEDs. *J. Mater. Chem. C* **2013**, *1*, 463−469.
(32) Nasu, K.; Nakagawa, T.; Nomura, H.; Lin, C. J.; Cheng, C. H.; Tseng, M. R.; Yasuda, T.; Adachi, C. A highly luminescent spiro-anthracenone-based organic light-emitting diode exhibiting thermally activated delayed fluorescence. *Chem. Commun.* **2013**, *49*, 10385−10387.
(33) Romain, M.; Tondelier, D.; Jeannin, O.; Geffroy, B.; Rault-Berthelot, J.; Poriel, C. Properties modulation of organic semiconductors based on a donor-spiro-acceptor (D-spiro-A) molecular design: new host materials for efficient sky-blue PhOLEDs. *J. Mater. Chem. C* **2015**, *3*, 9701−9714.
(34) Xue, L.; Cui, B.; Xie, S.; Yin, S. Influence of the Length of the Donor-Acceptor Bridge on Thermally Activated Delayed Fluorescence. *J. Phys. Chem. Lett.* **2019**, *10*, 302−308.
(35) Vikramaditya, T.; Saisudhakar, M.; Sumithra, K. Computational study on thermally activated delayed fluorescence of donor−linker−acceptor network molecules. *RSC Adv.* **2016**, *6*, 37203−37211.
(36) Park, I. S.; Seo, H.; Tachibana, H.; Kim, J. U.; Zhang, J.; Son, S. M.; Yasuda, T. Cyclohexane-Coupled Bipolar Host Materials with High Triplet Energies for Organic Light-Emitting Diodes Based on Thermally Activated Delayed Fluorescence. *ACS Appl. Mater. Interfaces* **2017**, *9*, 2693−2700.
(37) Liu, M.; Komatsu, R.; Cai, X.; Hotta, K.; Sato, S.; Liu, K.; Chen, D.; Kato, Y.; Sasabe, H.; Ohisa, S.; Suzuri, Y.; Yokoyama, D.; Su, S.-J.; Kido, J. Horizontally Orientated Sticklike Emitters: Enhancement of Intrinsic Out-Coupling Factor and Electroluminescence Performance. *Chem. Mater.* **2017**, *29*, 8630−8636.
(38) Kim, H. J.; Lee, C.; Godumala, M.; Choi, S.; Park, S. Y.; Cho, M. J.; Park, S.; Choi, D. H. Solution-processed thermally activated delayed fluorescence organic light-emitting diodes using a new polymeric emitter containing non-conjugated cyclohexane units. *Polym. Chem.* **2018**, *9*, 1318−1326.
(39) Ye, J.-T.; Wang, L.; Wang, H.-Q.; Pan, X.-M.; Xie, H.-M.; Qiu, Y.-Q. Effective Impact of Dielectric Constant on Thermally Activated Delayed Fluorescence and Nonlinear Optical Properties: Through-Bond/-Space Charge Transfer Architectures. *J. Phys. Chem. C* **2018**, *122*, 18850−18859.
(40) Takahashi, T.; Shizu, K.; Yasuda, T.; Togashi, K.; Adachi, C. Donor-acceptor-structured 1,4-diazatriphenylene derivatives exhibiting thermally activated delayed fluorescence: design and synthesis, photophysical properties and OLED characteristics. *Sci. Technol. Adv. Mater.* **2014**, *15*, No. 034202.
(41) Data, P.; Pander, P.; Okazaki, M.; Takeda, Y.; Minakata, S.; Monkman, A. P. Dibenzo[*a,j*]phenazine-Cored Donor−Acceptor−Donor Compounds as Green-to-Red/NIR Thermally Activated Delayed Fluorescence Organic Light Emitters. *Angew. Chem., Int. Ed.* **2016**, *55*, 5739−5744.
(42) Frisch, M. *GAUSSIAN09, Revision D01*; Gaussian Inc.: Pittsburgh, PA, 2009.
(43) Irfan, A.; Aftab, H.; Al-Sehemi, A. G. Push−pull effect on the geometries, electronic and optical properties of thiophene based dye-sensitized solar cell materials. *J. Saudi Chem. Soc.* **2014**, *18*, 914−919.
(44) Lu, J.; Zheng, Y.; Zhang, J. Tuning the color of thermally activated delayed fluorescent properties for spiro-acridine derivatives by structural modification of the acceptor fragment: a DFT study. *RSC Adv.* **2015**, *5*, 18588−18592.
(45) Hussain, A.; Yuan, H.; Li, W.; Zhang, J. Theoretical investigations of the realization of sky-blue to blue TADF materials via CH/N and H/CN substitution at the diphenylsulphone acceptor. *J. Mater. Chem. C* **2019**, *7*, 6685−6691.
(46) Wang, J.; Lu, J.; Zhang, J. Tuning the electronic and optical properties of diphenylsulphone based thermally activated delayed fluorescent materials via structural modification: A theoretical study. *Dyes Pigm.* **2017**, *143*, 42−47.
(47) Wang, L.; Li, T.; Feng, P.; Song, Y. Theoretical tuning of the singlet-triplet energy gap to achieve efficient long-wavelength thermally activated delayed fluorescence emitters: the impact of substituents. *Phys. Chem. Chem. Phys.* **2017**, *19*, 21639−21647.
(48) Freeman, D. M. E.; Musser, A. J.; Frost, J. M.; Stern, H. L.; Forster, A. K.; Fallon, K. J.; Rapidis, A. G.; Cacialli, F.; McCulloch, I.; Clarke, T. M.; Friend, R. H.; Bronstein, H. Synthesis and Exciton Dynamics of Donor-Orthogonal Acceptor Conjugated Polymers: Reducing the Singlet-Triplet Energy Gap. *J. Am. Chem. Soc.* **2017**, *139*, 11073−11080.
(49) Shao, S.; Hu, J.; Wang, X.; Wang, L.; Jing, X.; Wang, F. Blue Thermally Activated Delayed Fluorescence Polymers with Non-conjugated Backbone and Through-Space Charge Transfer Effect. *J. Am. Chem. Soc.* **2017**, *139*, 17739−17742.
(50) Lu, T.; Chen, F. Multiwfn: a multifunctional wavefunction analyzer. *J. Comput. Chem.* **2012**, *33*, 580−592.
(51) Duan, Y.-C.; Gao, Y.; Geng, Y.; Wu, Y.; Shan, G.-G.; Zhao, L.; Zhang, M.; Su, Z.-M. Towards red-light o-carborane derivatives with both aggregation induced emission and thermally activated delayed fluorescence combining quantum chemistry calculation with molecular dynamics simulation. *J. Mater. Chem. C* **2019**, *7*, 2699−2709.
(52) Shi, S.; Jung, M. C.; Coburn, C.; Tadle, A.; Sylvinson, M. R. D.; Djurovich, P. I.; Forrest, S. R.; Thompson, M. E. Highly Efficient Photo- and Electroluminescence from Two-Coordinate Cu(I) Complexes Featuring Nonconventional N-Heterocyclic Carbenes. *J. Am. Chem. Soc.* **2019**, *141*, 3576−3588.
(53) Liu, K.; Lalancette, R. A.; Jakle, F. Tuning the Structure and Electronic Properties of B-N Fused Dipyridylanthracene and Implications on the Self-Sensitized Reactivity with Singlet Oxygen. *J. Am. Chem. Soc.* **2019**, *141*, 7453−7462.
(54) Bibi, S.; Shafiq ur, R.; Jia, R.; Zhang, H.-X.; Bai, F.-Q. Effect of different topological structures (D-π-D and D-π-A-π-D) on the optoelectronic properties of benzo[2,1-B:3,4-B́]dithiophene based donor molecules toward organic solar cells. *Sol. Energy* **2019**, *186*, 311−322.
(55) Gupta, A. K.; Kumar, A.; Singh, R.; Devi, M.; Dhir, A.; Pradeep, C. P. Facile Synthesis of an Organic Solid State Near-Infrared-Emitter with Large Stokes Shift via Excited-State Intramolecular Proton Transfer. *ACS Omega* **2018**, *3*, 14341−14348.
(56) O'Boyle, N. M.; Tenderholt, A. L.; Langner, K. M. cclib: a library for package-independent computational chemistry algorithms. *J. Comput. Chem.* **2008**, *29*, 839−845.
(57) Mulliken, R. S. Electronic Population Analysis on LCAO−MO Molecular Wave Functions. I. *J. Chem. Phys.* **1955**, *23*, 1833−1840.
(58) Bickelhaupt, F. M.; van Eikema Hommes, N. J. R.; Fonseca Guerra, C.; Baerends, E. J. The Carbon−Lithium Electron Pair Bond in (CH3Li)n (n = 1, 2, 4). *Organometallics* **1996**, *15*, 2923−2931.
(59) Reed, A. E.; Weinstock, R. B.; Weinhold, F. Natural population analysis. *J. Chem. Phys.* **1985**, *83*, 735−746.
(60) Franceschetti, A.; Zunger, A. Direct Pseudopotential Calculation of Exciton Coulomb and Exchange Energies in Semiconductor Quantum Dots. *Phys. Rev. Lett.* **1997**, *78*, 915−918.
(61) Cao, Y.; Parker, I. D.; Yu, G.; Zhang, C.; Heeger, A. J. Improved quantum efficiency for electroluminescence in semiconducting polymers. *Nature* **1999**, *397*, 414−417.
(62) Baldo, M.; Segal, M. Phosphorescence as a probe of exciton formation and energy transfer in organic light emitting diodes. *Phys. Status Solidi A* **2004**, *201*, 1205−1214.
(63) Li, Y.; Zou, L.-Y.; Ren, A.-M.; Feng, J.-K. Theoretical study on the electronic structures and photophysical properties of a series of dithienylbenzothiazole derivatives. *Comput. Theor. Chem.* **2012**, *981*, 14−24.
(64) Seo, J. H.; Jin, Y.; Brzezinski, J. Z.; Walker, B.; Nguyen, T. Q. Exciton binding energies in conjugated polyelectrolyte films. *ChemPhysChem* **2009**, *10*, 1023−1027.
(65) Shang, X.; Wan, N.; Han, D.; Zhang, G. A theoretical study on the injection, transport, absorption and phosphorescence properties of heteroleptic iridium(III) complexes with different ancillary ligands. *Photochem. Photobiol. Sci.* **2014**, *13*, 574−582.

https://doi.org/10.1021/acsomega.3c01098
ACS Omega 2023, 8, 15638−15649

(66) Coropceanu, V.; Cornil, J.; da Silva Filho, D. A.; Olivier, Y.; Silbey, R.; Brédas, J.-L. Charge Transport in Organic Semiconductors. *Chem. Rev.* **2007**, *107*, 926−952.
(67) Nan, G.; Yang, X.; Wang, L.; Shuai, Z.; Zhao, Y. Nuclear tunneling effects of charge transport in rubrene, tetracene, and pentacene. *Phys. Rev. B: Condens. Matter Mater. Phys.* **2009**, *79* (), DOI: 10.1103/PhysRevB.79.115203.
(68) Hush, N. S. Adiabatic Rate Processes at Electrodes. I. Energy-Charge Relationships. *J. Chem. Phys.* **1958**, *28*, 962−972.
(69) Marcus, R. A. Electron transfer reactions in chemistry. Theory and experiment. *Rev. Mod. Phys.* **1993**, *65*, 599−610.
(70) Hutchison, G. R.; Ratner, M. A.; Marks, T. J. Hopping Transport in Conductive Heterocyclic Oligomers: Reorganization Energies and Substituent Effects. *J. Am. Chem. Soc.* **2005**, *127*, 2339−2350.
(71) Lobanova Griffith, O.; Gruhn, N. E.; Anthony, J. E.; Purushothaman, B.; Lichtenberger, D. L. Electron Transfer Parameters of Triisopropylsilylethynyl-Substituted Oligoacenes. *J. Phys. Chem. C* **2008**, *112*, 20518−20524.
(72) Wang, L.; Nan, G.; Yang, X.; Peng, Q.; Li, Q.; Shuai, Z. Computational methods for design of organic materials with high charge mobility. *Chem. Soc. Rev.* **2010**, *39*, 423−434.
(73) Gruhn, N. E.; da Silva Filho, D. A.; Bill, T. G.; Malagoli, M.; Coropceanu, V.; Kahn, A.; Brédas, J.-L. The Vibrational Reorganization Energy in Pentacene: Molecular Influences on Charge Transport. *J. Am. Chem. Soc.* **2002**, *124*, 7918−7919.

https://doi.org/10.1021/acsomega.3c01098
ACS Omega 2023, 8, 15638−15649